Pharmaceutical Research, Vol. 26, No. 1, January 2009 (© 2008)
DOI: 10.1007/s11095-008-9704-2

Research Paper

Enhanced Core Hydrophobicity, Functionalization and Cell Penetration of Polybasic Nanomatrices

Omar Z. Fisher,[1] Timothy Kim,[1] Stephen R. Dietz,[1] and Nicholas A. Peppas[1,2,3,4]

Received June 23, 2008; accepted August 5, 2008; published online August 28, 2008

Purpose. In this work a novel pH-responsive nanoscale polymer network was investigated for potential applications in nanomedicine. These consisted of a polybasic core surface stabilized with poly(ethylene glycol) grafts. The ability to control swelling properties via changes in core hydrophobicity and crosslinking feed density was assessed. The nanomatrices were also evaluated *in vitro* as nanocarriers for targeted intracellular delivery of macromolecules.
Materials and Methods. Photo-emulsion polymerization was used to synthesize poly[2-(diethylamino) ethyl methacrylate-co-*t*-butyl methacrylate-g-poly(ethylene glycol)] (PDBP) nanomatrices. These were characterized using NMR, dynamic and electrophoretic light scattering, electron microscopy. The cytocompatibility and cellular uptake of nanomatrices was measured using the NIH/3T3 and A549 cell lines.
Results. PDBP nanomatrices had a dry diameter of 40–60 nm and a hydrodynamic diameter of 70–90 nm in the collapsed state. Maximum volume swelling ratios from 6–22 were obtained depending on crosslinking feed density. Controlling the hydrophobicity of the networks allowed for control over the critical swelling pH without a significant loss in maximal volume swelling. The effect of PDBP nanomatrices on cell viability and cell membrane integrity depended on crosslinking feed density. Cell uptake and cytosolic delivery of FITC-albumin was enhanced from clathrin-targeting nanocarriers. The uptake resulted in nuclear localization of the dye in a cell type dependent fashion.
Conclusions. The results of this work indicate that PDBP nanomatrices have tunable swelling properties. The networks were cytocompatible and proved to be suitable agents for intracellular delivery.

KEY WORDS: cell uptake; endosomolytic agent; nanogel; pH-responsive; photopolymerization.

INTRODUCTION

The emergence and growth of nanomedicine has spurred the development of a wide variety of nanostructured devices for the treatment and detection of disease. As biomaterials these new devices must meet minimum standards of biocompatibility as well as possess advanced functionality. Ideally they should also be durable, fabricated with scalable processing methods and possess tunable properties. Photopolymerized polymer networks have been proven to meet all these criteria as macroscale biomaterials, and could potentially do the same on the nanoscale. This work was an attempt to further evaluate a novel photopolymerized hydrogel for applications in nanomedicine.

Nanogels are platform technologies with diverse biomedical applications. They can be tailor made for imaging, biosensing, therapeutic delivery, biomolecular recognition or multimodal purposes. Because they are covalently crosslinked, they have integrity that cannot be achieved in purely self-assembled systems. They can be easily fabricated on the nanoscale using diverse techniques such as nanolithography, nanofluidics, emulsions or the principles of self-assembly (1).

Much of the biomedical work on synthetic nanoscale polymers has centered on self-assembled systems such as liposomes or biodegradable thermoplastics such as poly(lactic-co-glycolic acid) or polyanhydrides for drug delivery. These systems can be loaded with drugs with low aqueous solubility and locally delivered to target tissue. Macromolecular therapeutics, such as nucleic acids or proteins, present additional challenges in drug delivery. These compounds are typically water soluble and degraded in the harsh processing conditions used to fabricate

[1] Department of Biomedical Engineering, The University of Texas at Austin, Austin, Texas 78752, USA.
[2] Department of Chemical Engineering, The University of Texas at Austin, 1 University Station C0400, Austin, Texas 78712-1062, USA.
[3] Division of Pharmaceutics, The University of Texas at Austin, Austin, Texas 78752, USA.
[4] To whom correspondence should be addressed. (e-mail: peppas@che.utexas.edu)

ABBREVIATIONS: AEM, 2-aminoethyl methacrylate hydrochloride; BFA, brefeldin A; BMA, tert-butyl methacrylate; DEAEM, 2-(diethylamino)ethyl methacrylate); DLS, dynamic light scattering; FITC, fluorescein isothiocyanate; HPLC, high performance liquid chromatography; LDH, lactate dehydrogenase; MyTAB, myristyltrimethylammonium bromide; PDBP, poly[2-(diethylamino) ethyl methacrylate-co-t-butyl methacrylate-g-poly(ethylene glycol)]; PDEAEM, poly[2-(diethylamino)ethyl methacrylate]; PDGP, poly[2-(diethylamino)ethyl methacrylate-g-poly(ethylene glycol)]; PEGMMA, poly(ethylene glycol) monomethyl ether monomethacrylate; RGDS, arginine-glycine-aspartate-serine; TEGDMA, Tetraethylene glycol dimethacrylate; Tf, holo-transferrin.

many synthetic polymer nanocarriers. Aqueous phase biomacromolecules can be encapsulated into hydrogels by simple partitioning. Also, networks can be made to respond to a range of environmental stimulus, such as pH, light, or temperature.

Photopolymerized poly[2-(diethylamino)ethyl methacrylate-g-poly(ethylene glycol)] (PDGP) nanomatrices are novel polymer networks that undergo a pH-dependent hydrophobe-to-hydrophile phase shift (2–3,6). This unique property qualifies these polymer matrices as nanogels only at low pH. It also makes these networks useful for the delivery of a wider variety of compounds including small lipophilic drugs as well as large biomolecules. These nanomatrices can be fabricated using free radical oil-in-water emulsion polymerization. They have been used as drug and gene delivery agents as well as platforms for the synthesis of nanocomposites (2,3, Fisher and Peppas, submitted).

The biocompatibility of PDGP nanostructures can be tuned by modifying surface and bulk properties. Polybasic polymers with conjugated poly(ethylene glycol) (PEG) chains are known to have increased biocompatibility both *in vivo* and *in vitro* (4,5). On PDGP nanogels the length of surface grafted PEG chains (2) as well as crosslinking feed density (Fisher and Peppas, submitted) were shown to modulate cytocompatibility *in vitro*. As the crosslinking feed density increases the network provides increased resistance to swelling forces and thereby a decreased pH needed to swell. Another strategy to lower the critical swelling pH is to increase the hydrophobicity of the matrix core (6). In this work PDGP networks were fabricated with enhanced core hydrophobicity to determine the effect on swelling properties, cytocompatibility and cell uptake.

MATERIALS AND METHODS

List of Reagents

The reagents 2-(diethylamino)ethyl methacrylate (DEAEM), *tert*-butyl methacrylate (BMA), 2-aminoethyl methacrylate (AEM), tetraethylene glycol dimethacrylate (TEGDMA), poly(ethylene glycol) monomethyl ether monomethacrylate (Mn=2,080, 50 wt.% aqueous solution) (PEGMMA), Brij-30, myristyltrimethylammonium bromide (MyTAB), fluorescein labeled bovine serum albumin (FITC-albumin_ and fluorescamine were all obtained from Sigma-Aldrich Corporation. Brefeldin A (BFA), deuterium chloride (DCl; 20% in D_2O), hydrochloric acid 1 N solution (HCl), sodium hydroxide 1 N solution (NaOH), fetal bovine serum (FBS) and calf serum (CS) were obtained from Thermo-Fisher Scientific Inc. Irgacure® 2959 was obtained from Ciba Chemical Company. Dulbecco's Modified Eagles Media (DMEM), non-essential amino acids, and antibiotic/antimycotics were obtained from Mediatech Inc. NIH/3T3 mouse fibroblasts and A549 human lung carcinoma cells were obtained from ATCC. Deuterium oxide (D_2O) was obtained from Cambridge Isotope Laboratories Inc. (Andover, MA, USA).

Polymer Synthesis

Polymerr nanomatrices were polymerized by photo-emulsion polymerization as described below. All monomers were passed through a column of basic alumina powder to remove inhibitor prior to use. In a round bottom flask, a mixture of TEGDMA, DEAEM and BMA was added to an aqueous solution of 5 wt.% PEGMMA, Irgacure 2959 at 0.5 wt.% of total monomer, 1.144 mg/mL MyTAB, and 4 mg/mL Brij-30 in deionized distilled water (ddH_2O). TEGDMA was used at mole feed ratios of 0.01, 0.025, 0.05, 0.10. The DEAEM content was kept constant at 5 wt% monomer in water and BMA was used at 20 mol% of DEAEM. For NMR studies uncrosslinked poly[2-(diethylamino)ethyl methacrylate] (PDEAEM) homopolymer, PDGP and poly[2-(diethylamino) ethyl methacrylate-co-t-butyl methacrylate-g-poly(ethylene glycol)] (PDBP) copolymers were prepared using the same conditions but without TEGDMA. Nanomatrices with primary amines were prepared with 5 mol% of total monomer content. AEM was dissolved in aqueous phase just prior to the reaction.

The mixture was emulsified for 10 min using a Misonix Ultrasonicator (Misonix Inc., Farmingdale, NY, USA) at 88 W while partially submerged in a stirred ice water bath. The emulsion was then purged with nitrogen gas for ten minutes, capped, and then exposed to a UV light source (Dymax BlueWave™ 200 UV, Dymax, Torrington, CT, USA) for 2.5 h at 140 mW/cm^2 with the light guide directed at the top of the emulsion, all with constant stirring.

The removal of unreacted reagents and surfactants was performed by repeatedly inducing polyeletrolyte-to-ionomer collapse. First, the pH of the suspension was lowered to 3 using 1 N HCl. Then acetone was added to 70 vol.%. This caused destabilization of the suspension followed by flocculation and sedimentation. The supernatant containing unreacted reagents and surfactants was separated by centrifuging the sediment into a pellet at 3,200 rcf. Following this, the pellet was resuspended in 0.5 N HCl and the process repeated four more times. The final centrifugation was followed by resuspension in ddH_20 and lyophilization. Nanomatrices were stored dry and desiccated in this protonated form until use.

^{1}H-NMR Spectroscopy

The BMA and PEG content were determined using ^{1}H NMR spectroscopy. Uncrosslinked polymers were dissolved in D_2O in 0.1 N DCl and NMR spectra were recorded using a 300 MHz Varian Unity+ 300 s spectrometer. The integrated intensity of the methylamine proton peak at 3.2 ppm was compared to the *tert*-butyl peak from BMA at 1.3 ppm, and the oxyethylene proton peak from the PEGMMA grafts at 3.6 ppm.

Scanning Electron Microscopy

Nanomatrices were imaged using a LEO 1530 scanning electron microscope (SEM). Dried nanomatrices were resuspended in ddH_20 and combined with 2 week old colloidal gold. The suspension was dried on an aluminum stage prior to imaging. Au colloid, with particle diameters between 1 and 3 nm, was prepared as described by Duff and coworkers (7). Average diameters in the dry state were obtained by digitally fitting transverse lines across a minimum of 30 particles, from three independent images, and comparing pixel lengths to the scale bar.

Light Scattering

The hydrodynamic diameter in aqueous suspension and effective surface ζ-potential of the polymer networks were

measured using a Brookhaven ZetaPlus instrument (Brookhaven Instruments Corp.) operating with a 659 nm diode laser source. Dynamic Light Scattering (DLS) measurements of particle size were conducted as follows: Dry particles were resuspended at 1 mg/mL in ddH_2O and brought up to final volume in 1× PBS with a 10× PBS. The same was then diluted with PBS to attain a scattering intensity between 200–800 kcps. The suspension pH was adjusted to 10 using microliter amounts of 1 N NaOH and gradually lowered using small amounts of 1 N HCl. Each measurement was taken in sestuplicate at room temperature.

Electrophoretic light scattering measurements of the surface ζ-potential were taken from nanomatrices suspended in 5 mM sodium phosphate at pH 7.4. All measurements were taken at 22°C with a scattering angle of 15°.

Bioconjugation

The primary amine content of functionalized nanomatrices was quantified using a fluorescamine assay. The fluorescence intensity from aqueous nanomatrix suspensions at 0.3 mg/mL was compared to AEM standard solutions.

For conjugation, 2 mg/mL suspensions of functionalized and non-functionalized particles were prepared in PBS with pH adjusted to 7.6. Either RGDS (American Peptide Company Inc.) or human holo-transferrin (Tf, Sigma-Aldrich Corporation) concentrates were added to the suspension to a final protein-amine mole ratio of 1:10. EDC and sulfo-NHS were used at 20× the protein molarity and 5 mM, respectively. The reaction proceeded for 1 hr, in the dark at room temperature while stirring. Conjugation was verified by high performance liquid chromatography (HPLC) of suspension filtrates passed through a 0.02 μm syringe filter. After reaction, the suspensions were dialyzed against 4°C PBS for 48 h, with the wash solution changed twice daily.

Cell Culture

NIH/3T3 murine fibroblasts were grown on 75 cm^2 tissue culture flasks in DMEM with 10% CS, 100 U/mL penicillin, and 100 μg/mL streptomycin. A549 human lung carcinoma cells were maintain in DMEM with 4.5 g/L glucose and L-glutamine, 1% non-essential amino acids, 100 U/mL penicillin, 100 μg/mL streptomycin and 10% FBS. The cells were kept at 37°C in a humidified incubator with 5% CO_2.

Cytocompatibility

NIH/3T3 cells were seeded in 96-well plates at 2,500 cells/cm^2 and grown to 85–90% confluency. A volume of 200 μL of fresh media was placed in each well 1 h before experimentation. Particle suspensions were prepared in PBS. A volume of 50 μL of each suspension was placed in each well, each plate was then shaken for 30 s at 550 rpm atop a thermomixer (Eppendorf), and incubated for 24 h. The media was then removed and used to quantify lactate dehydrogenase leakage (LDH) using a resazurin based fluorometric assay (Cytotox-ONE™ Homogeneous Membrane Integrity Assay, Promega Corp.). To measure cell metabolic activity the media was replaced with a standard MTS assay solution (CellTiter 96 AQueous, Promega Corp.) and incubated for 90 min. The fluorescence (560 nm excitation, 590 nm emission) and absorbance at 490 nm were measured using a microplate reader (Synergy HT, BioTek Instruments, Inc.).

Cell Uptake

Transferrin conjugated, RGDS conjugated and control nanomatrices were resuspended in PBS at 1 mg/mL. They were then combined with an equal volume of FITC-albumin solution at 0.5 mg/mL and the pH adjusted to 6.5 using 1 N HCl. The mixtures were stirred for 30 min at room temperature. The carriers were collapsed by raising the pH to 7.4 using 1 N NaOH. Samples of each suspension were passed through a 0.02 μm syringe filter and analyzed using HPLC. Complete loading of the fluorescently labeled protein into the nanomatrices was confirmed by comparing the filtrate to a standard solution at 0.25 mg/mL.

NIH/3T3 cells were seeded in 96-well plates at 2,500 cells/cm^2 and grown to 85–90%. One hour prior to uptake experiments the media was replaced with 160 μL fresh media. FITC-albumin loaded nanomatrix suspensions were added at a volume of 40 μL to each well to a final concentration of 100 μg/mL. Prior to adding to cell wells, BFA was added to certain suspensions to obtain a final well concentration of 5 μg/mL. A 150 mg/mL solution of RGDS in PBS was added to the appropriate suspensions at 100× conjugated peptide. Control wells received 40 μL of PBS. The suspensions were allowed to incubate for 1 hr, rinsed twice with warm PBS then FITC fluorescence measured using a microplate reader.

A549 cells were seeded in 96-well plates at 14,000 cells/cm^2 and grown to confluency. For uptake experiments the same procedure was followed as for NIH/3T3's.

An F test was used to determine if each experimental group had a significantly different variance from the control ($p<0.05$). Given the results of the F test, a Student's t test was used, assuming either equal or unequal variances, to determine if each experimental group mean was significantly different from the control group mean.

Optical Microscopy

A549 and NIH/3T3 cells were grown on eight-well chamber slides under the same conditions used for uptake measurements. After the 1 hr exposure to nanomatrix suspensions the slides were rinsed in warm PBS and fixed in 10% buffered formalin for 15 min. They were then rinsed in water, stained with DAPI, rinsed again and dried at room temperature. Images were taken with a Nikon ME600 microscope using reflected light and epifluorescence and overlayed using MetaMorph® Imaging Software.

RESULTS AND DISCUSSION

Nanomatrix Characterization

Poly[2-(diethylamino)ethyl methacrylate-co-*t*-butyl methacrylate] nanomatrices surface grafted with poly(ethylene glycol) chains (PDBP) were successfully prepared using UV-initiated photo-emulsion polymerization. The reactions went to 60–67% conversion, based on mass yield, and resulted in fairly monodisperse spherical nanostructures 51±7 nm in diameter. In the pH range 7.4–7.55 the suspended particles were all 71–73 nm in diameter except for the lowest crosslinking feed density which was 90 nm in diameter (Fig. 1).

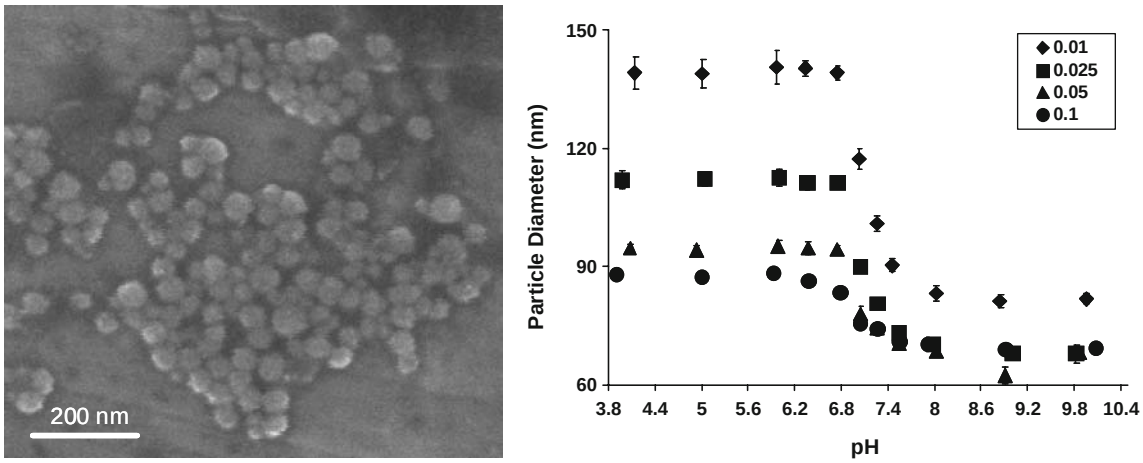

Fig. 1. *Left* Scanning electron microscope image of PDBP nanomatrices. *Right* The diameters of nanomatrices suspended in PBS over a range of pH values. Four different crosslinking feed ratios are shown. The data is expressed as the mean± standard deviation (n=6).

Using the collapsed diameters from SEM measurements, the maximum volume swelling ratio can be computed for the nanogels at four different crosslinking mole feed ratios as

$$Q = \frac{d_s^3}{d_d^3} \tag{1}$$

where d_s and d_d are the particle diameters in the swollen state and dry state, respectively. The average maximum swelling ratios (±standard deviation, n=6) were 22±1, 12±0.04, 7±0.2, and 6±0.1 for crosslinking mole feed ratios of 0.01, 0.025, 0.05 and 0.10 respectively. In all cases maximal swelling was reached at a pH of 6.75 and lower. These swelling ratios were essentially the same as those obtained for PDGP nanomatrices, suggesting that the same constraints on encapsulation apply. This was investigated by the encapsulating of both insulin and bovine serum albumin (BSA), which both had 100% loading efficiency in PDBP networks with 2.5% crosslinking feed density. This is higher than what could be loaded into PDGP nanomatrices which entrapped only 27.7% BSA and 83.1% insulin at the same crosslinking feed ratio. This suggests that the more hydrophobic network is more efficient at trapping compounds at physiological pH.

From the volume swelling plot it is clear that by varying crosslinking feed density and hydrophobicity the swelling properties of the networks can be controlled. (Fig. 2). The increased core hydrophobicity also had the effect of tightening the loosely crosslinked networks in the collapsed state. The 1% crosslinked PDGP collapsed to a much lesser extent than PDBP. PDEAEM homopolymer is insoluble in water above its pK_a yet is known to take on some water (8), due to the high density of hydrogen bond accepting amines. The additional lipophilic units allow the network to exclude more water in the collapsed state.

The incorporation of *t*-BMA into the network was verified and quantified using proton NMR (Fig. 3). The spectra show a new peak at 1.3 ppm corresponding to the *tert*-butyl groups. The *t*-BMA/DEAEM mole ratio in the polymer was 30 mol% of the DEAEM fraction as obtained by comparing the *tert*-butyl peak area with the methylamine peak at 3.2 ppm. The PEG/DEAEM mole ratio was 4%. When the PEG fraction calculated from NMR and polymer yield are taken into account the bulk of unreacted monomer is mostly unreacted PEGMMA grafts. The lipophilic comonomers all go to near complete conversion.

The use of polyamines is known to enhance cellular adhesion of biomaterials (9). The cell membrane glycocalyx is a molecular forest of branched, highly sulfated proteoglycans, which are strongly attracted to polycations (10–13). For macroscale materials this can lead to an enhanced biological interface. For nanoscale biomaterials this can lead to increased toxicity due to cell lysis. As a PDEAEM based, material PDBP could affect cellular membranes in the same way as the similar tertiary amine methacrylate polymer poly [2-(dimethylamino)ethyl methacrylate]. This polymer was shown to cause red blood cell lysis and *in vivo* toxicity (14). The potential for damage is dependent on the amount of charge available at the polymer surface. zeta-potential measurements taken at physiological pH showed a slight decline in surface charge as crosslinking feed density increased. The average values (±SD, n=10) were 3.8±6 mV

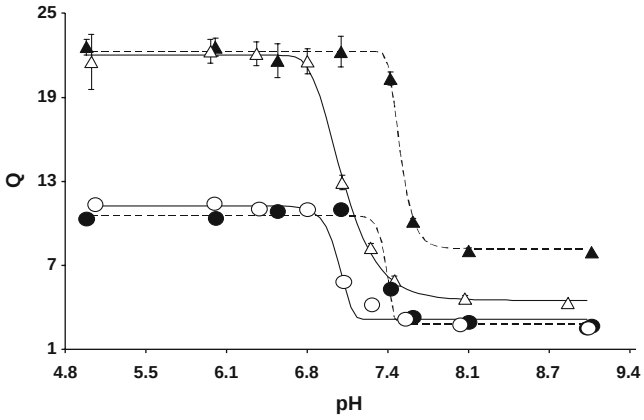

Fig. 2. Volume swelling ratios *vs* pH for PDGP nanomatrices with crosslinking mole feed densities of 1% (*filled triangle*) and 2.5% (*filled circle*) and PDBP nanomatrices with densities of 1% (*empty triangle*) and 2.5% (*empty circle*). The *curves* represent best Gompertz fits for the PDBP (*solid lines*) and PDGP (*dashed lines*) data. Data points are represented by the mean with errors equal to ±standard deviation (n=6).

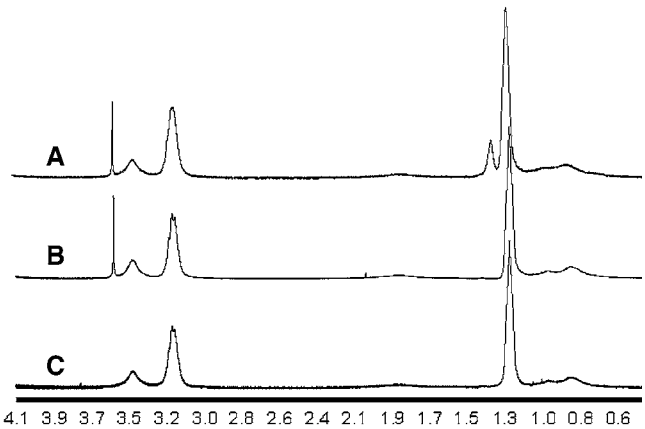

Fig. 3. ^{1}H NMR spectra for uncrosslinked PDBP (**A**), PDGP (**B**) and PDEAEM homopolymer (**C**).

at 1% crosslinking mole feed density, 3.9±4 mV at 2.5%, 1.3± 3.6 mV at 5% and 0.9±3.4 mV. None of the nanostructures were significantly cationized, especially when compared with the 15–30 mV zeta-potentials needed for other polybasic carriers to induce nonspecific cell uptake (15–17).

Cell Viability

Wolff and Rozema (18) described the positive surface charge on most intracellular delivery agents as a 'double edged sword,' required for uptake yet responsible for significant toxicity. The amount of surface charge of a polybasic material is related to the pK_a of the ionizable groups. The gold standard in intracellular delivery, polyethyleneimine (PEI), has a pK_a of 5.5, leaving only about one sixth of the available amines protonated at physiological pH (19) yet it can reduce cell viability by up to 85% (20). PDEAEM has a pK_a of 7.3–7.5 (19). PDBP appeared to have a maximum buffering capacity at pH values only slightly below this, meaning that it has potentially much greater cationization than PEI at physiological pH. To determine how this affected toxicity, *in vitro* cytocompatibility was measured using confluent NIH/3T3 fibroblasts exposed to PDBP nanomatrix suspensions for 24 h. The viability of these cell monolayers was measured using a metabolic cell viability assay complexed with a cytotoxicity assay which measured LDH leakage from damaged cell membranes.

The two assays provided different assessments of cell-material response. The concentration range of 0.125–1 mg/mL chosen was to obtain an upper limit on cytocompatibility. When concentrations in the 1–20 μg/mL range were used, typical for polyplex gene delivery carriers, no toxicity was detected. Based on the metabolic assay, the two lowest crosslinking mole feed densities show moderate to severe cytotoxicity above 0.25 mg/mL, while the other samples show no cytotoxicity at any concentration (Fig. 4A). Exposure to PDBP for 24 h had much less effect on cell metabolism than PDGP exposure for 2 h data not shown). The reason for this is most likely the lower critical swelling pH. This has a twofold effect: it decreases cationization and increases PEG surface graft density by tightening the networks. Increased crosslinking feed density would have the same effect on surface graft density.

A different relationship between crosslinking feed density and cytocompatibility was obtained from looking at the LDH leakage assay (Fig. 4B). The results showed that the 10% crosslinked sample had the only insignificant effect on plasma membrane integrity, and only below 0.25 mg/mL ($P<$ 0.05). The membrane damage at higher concentrations appeared negligible. At 5% crosslinking feed density the carriers caused moderate membrane leakage above 0.25 mg/mL and a small amount of membrane disruption at lower concentrations. At the two lower crosslinking feed densities severe membrane disruption occurs that corresponds with the metabolic activity.

Taken together, the results of the two assays show that there is a certain degree of carrier induced membrane disruption that is either not harmful to cells or only transiently so. A short term, transient cytotoxicity would cause a detectable LDH leakage into the cell culture media. But, using

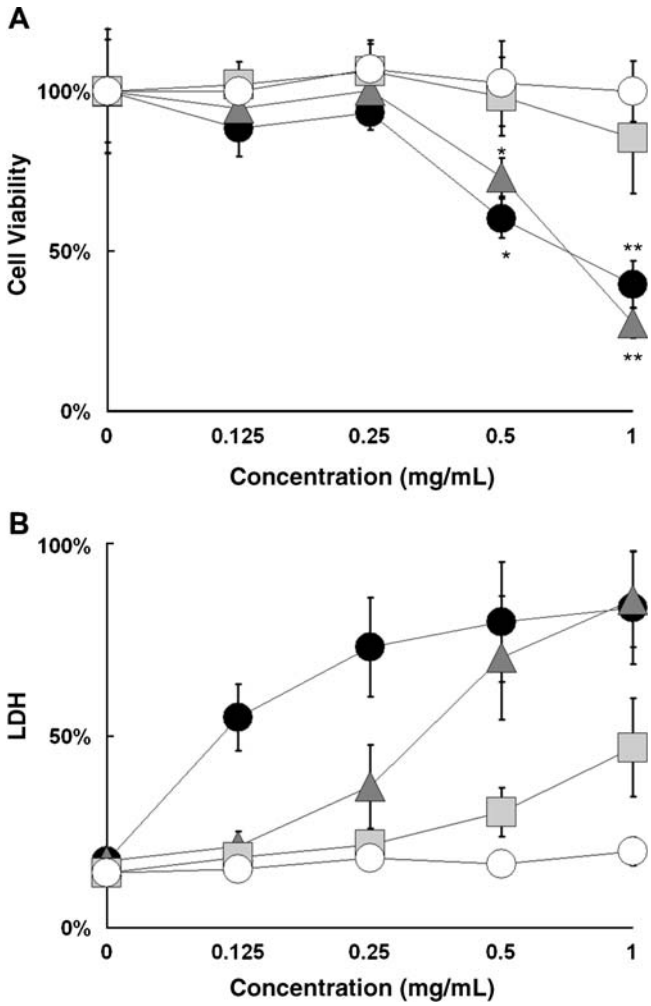

Fig. 4. Cytocompatibility of NIH/3T3 cells exposed to PDBP nanomatrices with crosslinking feed ratios of 0.01 (*filled circle*), 0.025 (*filled triangle*), 0.05 (*filled square*) and 0.1 (*empty circle*). **A** Cell viability measurements using a metabolic assay. Data is expressed as percentage of control viability. **B** Cytotoxicity measurements using an LDH leakage assay. Data is expressed as percentage of Triton X-100 (+)-control. Data is represented as mean±SD (n=6). *Asterisks* represent statistically significant difference from control (*P<0.05, **P<0.005).

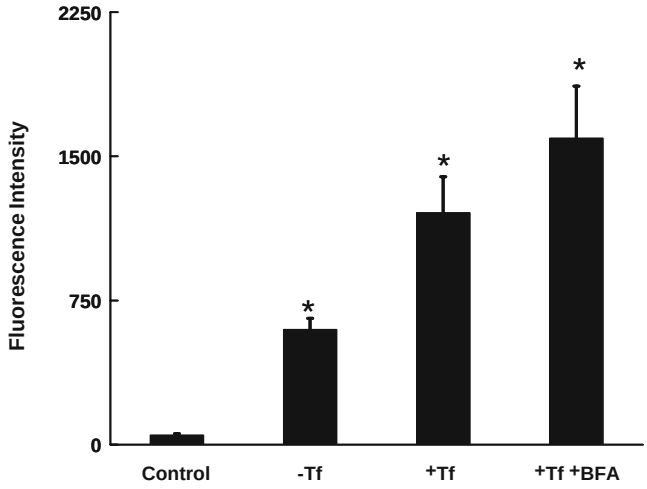

Fig. 5. FITC-albumin loaded nanomatrix uptake into A549 cells after 1 hr. Carriers without conjugated transferrin (−Tf), with (+Tf), and with transferrin co-delivered with BFA (+Tf +BFA) were used. Control cells were exposed to FITC-albumin alone at equal concentration. Each *bar* represents the mean±SD (n=8). Asterisks represent statistically significant difference from the control (*P<0.0005).

a cell viability assay, this effect could potentially be masked by new cell growth. This may be the reason that the two different cytocompatibility assays used here would provide different IC_{50} values. But the use of both was needed to verify that membrane damage was the primary cause of cytotoxicity.

Bioconjugation

To introduce specificity into the carrier it was first functionalized with primary amines by including AEM into the aqueous phase of the reaction. The presence of primary amines was confirmed and quantified using a fluorescamine assay. The measured amine content between three batches was consistently 26–27 μmol/g, representing a 16.9% incorporation efficiency. It is important to note that the monomer AEM worked well in this initial application but the use of it in other reaction schemes may be complicated by its tendency to quickly rearrange, resulting in a loss of primary amines (21). The polymerized form is stable. In this work it was added just prior to the reaction, helping to preserve more of the original structure. Also, the presence of any primary amines during the polymerization can lead to Michael addition.

There are different pathways by which nanoscale intracellular delivery agents have been shown to enter the cell. The availability of each pathway varies by cell type and particle size (15). Phagocytosis and macropinocytosis are both actin driven processes resulting in large endosomal compart-

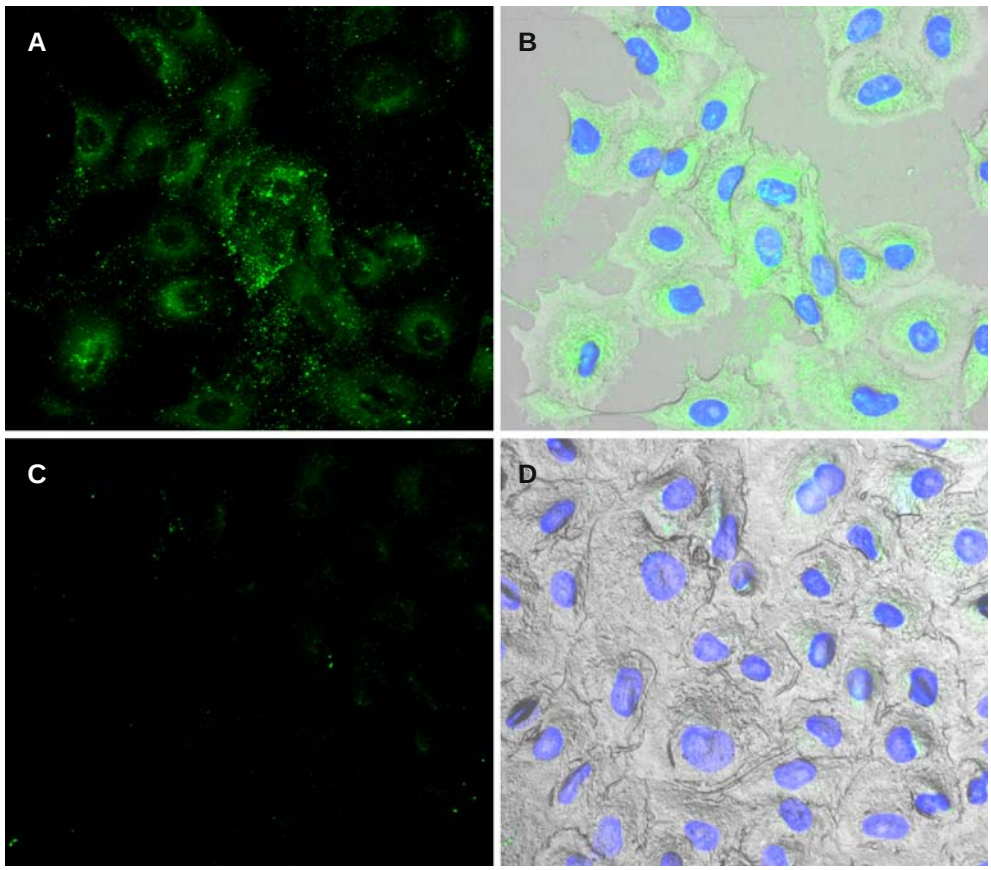

Fig. 6. **A**, **B** FITC-albumin delivered into A549 cells by PDBP-Tf conjugates 1 h. The intensity of the dye is mostly perinuclear. **C**, **D** Control A549 cells exposed to FITC-albumin solution.

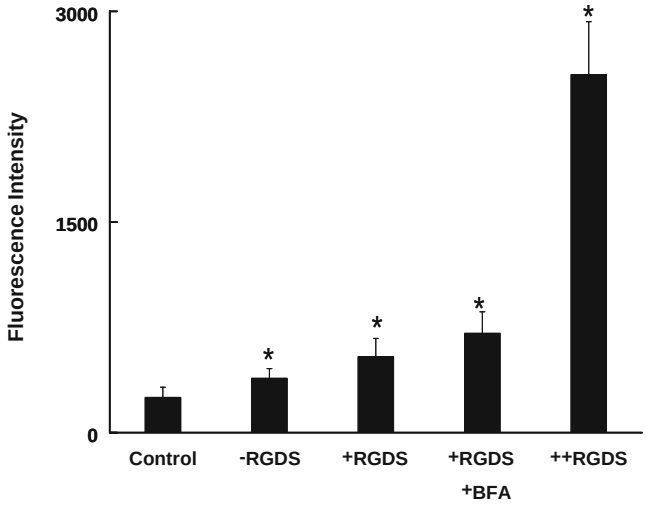

Fig. 7. FITC-albumin loaded nanomatrix uptake into NIH/3T3 cells after 1 h. Carriers without RGDS (−RGDS), conjugated (+RGDS), conjugated to RGDS co-delivered with BFA (+RGDS +BFA), and conjugates with 100× excess RGDS in solution. Control cells were exposed to FITC-albumin alone at equal concentration. Each bar represents the mean±SD (n=8). *Asterisks* represent statistically significant difference from the control (*P<0.0001).

ments (22). For carriers >200 nm these are the main pathways (23). Phagocytosis is normally limited to certain cell types, such as macrophages, that function to clear infections and debris, yet certain pathogens are able to induce phagocytosis in non-phagocytic cells (24). Macropinocytosis can be triggered by various growth factors, such as epidermal growth factor (25). This pathway can either result in lysosomal fusion or recycling to the cell membrane. Carriers below 200 nm can enter the cell through macropinocytosis, clathrin-coated pits, caveolin-dependent or lipid raft-dependent endocytosis. Uptake through caveolae or lipid rafts results in a neutral pH compartment (26), useless for an acid swellable carrier. Only entry via clathrin coated-pits is an assured way for a carrier to encounter the influx of protons responsible for the success of many polybasic cell delivery agents.

To target clathrin-coated pits PDBP nanomatrices were conjugated to human holo-transferrin using 1-ethyl-3-(3-dimethylaminopropyl) carbodiimide hydrochloride and sulfo-NHS. Elution fractions passed through a 0.02 μm filter confirmed no binding of Tf to nonfunctional, EDC/Sulfo-NHS treated controls while no Tf eluted from functional gels. Transferrin is known to be endocytosed through the clathrin-dependent pathway by cells (27). Vinogradov and coworkers (28,29) showed that transferrin conjugated nanogels could be used for tumor targeting and crossing the blood-brain barrier.

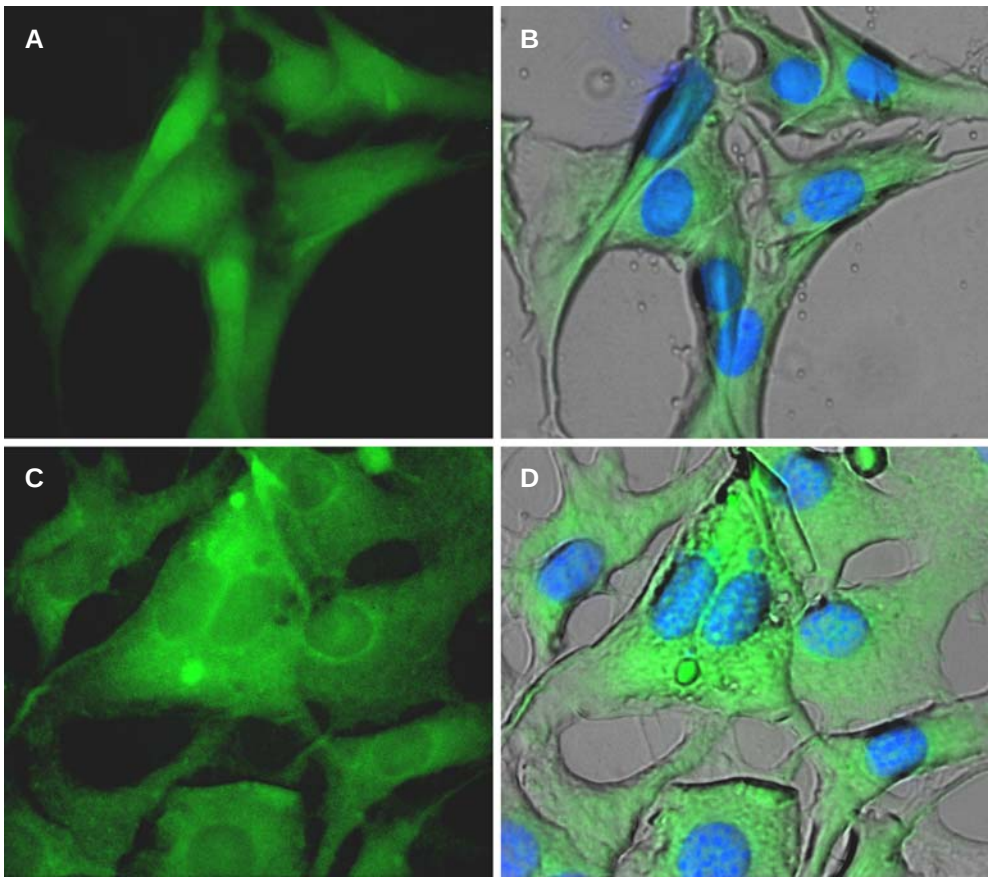

Fig. 8. **A**, **B** NIH/3T3 uptake of PDBP-RGDS conjugates loaded with FITC-albumin after 1 h. **C**, **D** Codelivery of BFA and PDBP-RGDS conjugates loaded with FITC-albumin. BFA appears to inhibit nuclear localization of the dye.

Ogris and coworkers (30) showed that transferrin conjugated PEG/PEI/DNA nanoparticles had targeting specificity with reduced serum protein adsorption. However, *in vivo* the circulation half-life was fairly short. This was likely due to the inherent instability of particles formed by polycomplexation.

A549 Cell Uptake

Cell uptake was investigated using the A549 human pulmonary epithelial cell line. FITC-albumin was loaded into the nanocarriers as an imaging probe and the fluorescence was quantified. The unconjugated carriers showed significant uptake compared to FITC-albumin alone (Fig. 5). In this case the unconjugated control carriers were functionalized with AEM to account for any non-specific uptake caused by free amines. Conjugation with transferrin approximately doubled the uptake of the carrier. Wan and coworkers (31) showed that treatment with BFA caused an increase in transferrin uptake in Madin–Darby canine kidney cells. To determine if it had the same effect on PDBP uptake it was co-delivered with them, resulting in a threefold increase in uptake. Interestingly, co-delivery of transferrin in solution had a similar effect (data not shown). During conjugation the transferrin-amine ratio was kept low, at 1:10, to limit protein-protein conjugation. Lim and Shen (32) showed that oligo-Tf resulted in greater cell uptake than monomeric Tf. This suggests that the bioconjugate ratio used here could be increased 30-fold without any reduction in the biological activity of transferrin.

Gene delivery carriers face the barrier of cell entry, endosomal escape and also the nuclear membrane. Inefficient release of nucleic acids from the carrier can inhibit the transfection efficiency of non-viral gene delivery agents. Fluorescence microscopy was used to look at the ability of PDBP nanomatrices to deliver FITC-albumin to the nucleus (Fig. 6). In A549 cells exposed PDBP-Tf conjugates fluorescence is strong in the vicinity around the nucleus but poor inside, similar to when nuclear pores are blocked with an antibody (33). The uptake and targeting potential of the carrier was clearly enhanced by transferrin conjugation. But the lack of nuclear dye localization leaves doubt about the release of payload into the cytosol.

There is a discrepancy in the literature on size exclusion limit of the nuclear pores. Some authors claim that compounds larger than 60 kDa can not cross through nuclear pores unassisted (34,35). Wang and Brattain (36) claim that much larger compounds, up to 110 kDa, pass through nuclear pore complexes passively. Bovine serum albumin, the 67 kDa compound chosen as a model drug in this work, is the molecule that set the 60 kDa limit in earlier work due to its inefficient entry through nuclear pores (37,38). Wang and Brattain also noted the inconsistency in nuclear pore size exclusion between cell types.

NIH/3T3 Cell Uptake

In order to account for cell type variability, PDBP nanomatrices were clathrin targeted for uptake in NIH/3T3 cells. First, the RGDS peptide sequence was conjugated to PDBP nanocarriers. The carrier was then loaded with FITC-albumin and incubated with NIH/3T3 fibroblasts. RGDS conjugation essentially made the nanocarriers viral mimics. Many adenoviruses use a pH-triggered endosomolysis to enter the cytosol of infected cells. To infect the cell they display an RGD sequence on their capsid surface to target specific integrins for clathrin mediated uptake (39,40).

All of the nanocarrier formulations displayed significantly higher uptake over the control solution (Fig. 7). Uptake was significantly increased with the use of RGD, and RGD with BFA. And in contrast to the A549 results the uptake caused nuclear localization of the dye in the murine fibroblasts. Despite the increase, when the BFA treated cells were viewed under the microscope there was mostly perinuclear fluorescence (Fig. 8). Brefeldin A is known to interfere with the formation of clathrin coats around endosomes (41). This may interfere with the endosome maturation, blocking the drop in pH required to swell the nanocarriers. The greatest enhancement was achieved by co-delivering soluble RGDS at a 100-fold excess. Instead of competing for binding the soluble peptide seemed to allow the nanocarrier to piggyback into the cell, similar to the result with transferrin.

CONCLUSIONS

The general nanoparticle size range for extended circulation half-life in the blood is between 50–200 nm in diameter (42). Tissue targeting can be achieved passively by tailoring nanoparticle size to exploit the enhanced permeation of pathological vasculature such as in tissue rheumatoid arthritis, tumorogenesis or infarction (43). pH-responsive nanostructures can also be used to target low pH compartments such as tumor tissue or intracellular compartments (44–48). PDGP nanomatrices are of the ideal size and possess the appropriate pH-responsiveness needed for these applications. This work has also shown that exploiting hydrophobicity along with crosslinking properties can make these properties tunable.

Polybasic endosomolytic agents can be uptaken into cells by nonspecific surface attraction, a process that is not well suited for *in vivo* applications and comes with significant toxicity. PDBP nanomatrices have been designed as surface neutralized proton sponges with very low cytotoxicity. Cell delivery agents that make use of the proton sponge effect are best targeted to cell uptake pathways that lead to lysosomes. This work showed that PDBP nanomatrices can be clathrin-targeted, making them useful as lysosomotropic drug delivery agents. Further work is needed to determine the efficacy of these structures *in vivo*.

ACKNOWLEDGEMENTS

The authors would like to acknowledge support from the National Institutes of Health, grant number EG-000246, a National Science Foundation Integrative Graduate Education and Research Traineeship (IGERT) Fellowship (to O.Z.F.), DGE-03-33080, and the University of Texas at Austin Undergraduate Research Fellowships to T.K. and S. R.D. The authors would also like to acknowledge the assistance of the University of Texas at Austin Institute for Cellular and Molecular Biology, the Texas Materials Institute and Professor Lisa Brannon-Peppas, Ph.D. for the use of their facilities.

REFERENCES

1. J. K. Oh, R. Drumright, D. J. Siegwart, and K. Matyjaszewski. The development of microgels/nanogels for drug delivery applications. *Prog. Polym. Sci.* **33**:448–477 (2008) doi:10.1016/j.progpolymsci.2008.01.002.
2. M. Oishi, H. Hayashi, K. Itaka, K. Kataoka, and Y. Nagasaki. pH-responsive PEGylated nanogels as targetable and low invasive endosomolytic agents to induce the enhanced transfection efficiency of nonviral gene vectors. *Colloid Polymer Sci.* **285**:1055–1060 (2007) doi:10.1007/s00396-007-1660-6.
3. H. Hayashi, M. Iijima, K. Kataoka, and Y. Nagasaki. pH-sensitive nanogel possessing reactive PEG tethered chains on the surface. *Macromolecules*. **37**:5389–5396 (2004) doi:10.1021/ma049199g.
4. M. Lee, and S. W. Kim. Polyethylene glycol-conjugated copolymers for plasmid DNA delivery. *Pharm. Res.* **22**:1–10 (2005) doi:10.1007/s11095-004-9003-5.
5. H. Petersen, P. M. Fechner, A. L. Martin, K. Kunath, S. Stolnik, C. J. Roberts, D. Fischer, M. C. Davies, and T. Kissel. Polyethylenimine-graft-poly(ethylene glycol) copolymers: influence of copolymer block structure on DNA complexation and biological activities as gene delivery system. *Bioconjug. Chem.* **13**:845–854 (2002) doi:10.1021/bc025529v.
6. R. A. Siegel, and J. M. Cornejo-Bravo. Hydrophobic polyelectrolytes—effect of hydrophobicity on buffering and colloid osmotic-pressure. *ACS Symp. Ser.* **480**:131–145 (1992).
7. D. G. Duff, A. Baiker, and P. P. Edwards. A new hydrosol of gold clusters. 1. Formation and particle-size variation. *Langmuir.* **9**:2301–2309 (1993) doi:10.1021/la00033a010.
8. J. M. Cornejo-Bravo, and R. A. Siegel. Water vapour sorption behaviour of copolymers of N,N-diethylaminoethyl methacrylate and methyl methacrylate. *Biomaterials*. **17**:1187–1193 (1996) doi:10.1016/0142-9612(96)84939-8.
9. A. Kishida, H. Iwata, Y. Tamada, and Y. Ikada. Cell behaviour on polymer surfaces grafted with non-ionic and ionic monomers. *Biomaterials*. **12**:786–792 (1991) doi:10.1016/0142-9612(91)90031-5.
10. A. Ziegler, P. Nervi, M. Durrenberger, and J. Seelig. The cationic cell-penetrating peptide CPP(TAT) derived from the HIV-1 protein TAT is rapidly transported into living fibroblasts: optical, biophysical, and metabolic evidence. *Biochemistry*. **44**:138–148 (2005) doi:10.1021/bi0491604.
11. O. Boussif, F. Lezoualch, M. A. Zanta, M. D. Mergny, D. Scherman, B. Demeneix, and J. P. Behr. A versatile vector for gene and oligonucleotide transfer into cells in culture and *in-vivo*—polyethylenimine. *Proc. Natl. Acad. Sci. U.S.A.* **92**:7297–7301 (1995) doi:10.1073/pnas.92.16.7297.
12. J. P. Behr. The proton sponge: A trick to enter cells the viruses did not exploit. *Chimia*. **51**:34–36 (1997).
13. A. Ziegler, and J. Seelig. Binding and clustering of glycosaminoglycans: a common property of mono- and multivalent cell-penetrating compounds. *Biophys. J.* **94**:2142–2149 (2008) doi:10.1529/biophysj.107.113472.
14. E. Moreau, M. Domurado, P. Chapon, M. Vert, and D. Domurado. Biocompatibility of polycations: *In vitro* agglutination and lysis of red blood cells and *in vivo* toxicity. *J. Drug Target.* **10**:161–173 (2002) doi:10.1080/10611860290016766.
15. K. von Gersdorff, N. N. Sanders, R. Vandenbroucke, S. C. De Smedt, E. Wagner, and M. Ogris. The internalization route resulting in successful gene expression depends on polyethylenimine both cell line and polyplex type. *Mol. Ther.* **14**:745–753 (2006) doi:10.1016/j.ymthe.2006.07.006.
16. K. A. Howard, U. L. Rahbek, X. D. Liu, C. K. Damgaard, S. Z. Glud, M. O. Andersen, M. B. Hovgaard, A. Schmitz, J. R. Nyengaard, F. Besenbacher, and J. Kjems. RNA interference *in vitro* and *in vivo* using a chitosan/siRNA nanoparticle system. *Mol. Ther.* **14**:476–484 (2006) doi:10.1016/j.ymthe.2006.04.010.
17. P. Erbacher, T. Bettinger, P. Belguise-Valladier, S. M. Zou, J. L. Coll, J. P. Behr, and J. S. Remy. Transfection and physical properties of various saccharide, poly(ethylene glycol), and antibody-derivatized polyethylenimines (PEI). *J. Gene Med.* **1**:210–222 (1999) doi:10.1002/(SICI)1521-2254(199905/06)1:3<210::AID-JGM30>3.0.CO;2-U.
18. J. A. Wolffand, and D. B. Rozema. Breaking the bonds: non-viral vectors become chemically dynamic. *Mol. Ther.* **16**:8–15 (2008) doi:10.1038/sj.mt.6300326.
19. S. C. De Smedt, J. Demeester, and W. E. Hennink. Cationic polymer based gene delivery systems. *Pharm. Res.* **17**:113–126 (2000) doi:10.1023/A:1007548826495.
20. N. Nishiyama, A. Iriyama, W. D. Jang, K. Miyata, K. Itaka, Y. Inoue, H. Takahashi, Y. Yanagi, Y. Tamaki, H. Koyama, and K. Kataoka. Light-induced gene transfer from packaged DNA enveloped in a dendrimeric photosensitizer. *Nat. Mater.* **4**:934–941 (2005) doi:10.1038/nmat1524.
21. J. M. Geurts, C. M. Gottgens, M. A. I. Van Graefschepe, R. W. A. Welland, J. J. G. Van Es, and A. L. German. Syntheses of new amino-functionalized methacrylates and their use in free radical polymerizations. *J. Appl. Polym. Sci.* **80**:1401–1415 (2001) doi:10.1002/app.1230.
22. M. Amyere, M. Mettlen, P. Van Der Smissen, A. Platek, B. Payrastre, A. Veithen, and P. J. Courtoy. Origin, originality, functions, subversions and molecular signalling of macropinocytosis. *Int. J. Med. Microbiol.* **291**:487–494 (2002) doi:10.1078/1438-4221-00157.
23. S. Grosse, Y. Aron, G. Thevenot, D. Francois, M. Monsigny, and I. Fajac. Potocytosis and cellular exit of complexes as cellular pathways for gene delivery by polycations. *J. Gene Med.* **7**:1275–1286 (2005) doi:10.1002/jgm.772.
24. S. Corr, C. Hill, and C. G. Gahan. An *in vitro* cell-culture model demonstrates internalin- and hemolysin-independent translocation of Listeria monocytogenes across M cells. *Microb. Pathog.* **41**:241–250 (2006).
25. M. A. West, M. S. Bretscher, and C. Watts. Distinct endocytotic pathways in epidermal growth factor-stimulated human carcinoma A431 cells. *J. Cell Biol.* **109**:2731–2739 (1989) doi:10.1083/jcb.109.6.2731.
26. L. Pelkmans, and A. Helenius. Endocytosis via caveolae. *Traffic*. **3**:311–320 (2002) doi:10.1034/j.1600-0854.2002.30501.x.
27. K. Miller, M. Shipman, I. S. Trowbridge, and C. R. Hopkins. Transferrin receptors promote the formation of clathrin lattices. *Cell*. **65**:621–632 (1991) doi:10.1016/0092-8674(91)90094-F.
28. S. V. Vinogradov. Colloidal microgels in drug delivery applications. *Curr. Pharm. Des.* **12**:4703–4712 (2006) doi:10.2174/138161206779026254.
29. S. V. Vinogradov, E. V. Batrakova, and A. V. Kabanov. Nanogels for oligonucleotide delivery to the brain. *Bioconjug. Chem.* **15**:50–60 (2004) doi:10.1021/bc034164r.
30. M. Ogris, S. Brunner, S. Schuller, R. Kircheis, and E. Wagner. PEGylated DNA/transferrin-PEI complexes: reduced interaction with blood components, extended circulation in blood and potential for systemic gene delivery. *Gene Ther.* **6**:595–605 (1999) doi:10.1038/sj.gt.3300900.
31. J. Wan, M. E. Taub, D. Shah, and W. C. Shen. Brefeldin A enhances receptor-mediated transcytosis of transferrin in filter-grown Madin-Darby canine kidney cells. *J. Biol. Chem.* **267**:13446–13450 (1992).
32. C. J. Lim, and W. C. Shen. Comparison of monomeric and oligomeric transferrin as potential carrier in oral delivery of protein drugs. *J. Control. Release.* **106**:273–286 (2005) doi:10.1016/j.jconrel.2005.05.001.
33. L. C. Trotman, N. Mosberger, M. Fornerod, R. P. Stidwill, and U. F. Greber. Import of adenovirus DNA involves the nuclear pore complex receptor CAN/Nup214 and histone H1. *Nat. Cell Biol.* **3**:1092–1100 (2001) doi:10.1038/ncb1201-1092.
34. B. Talcott, and M. S. Moore. Getting across the nuclear pore complex. *Trends Cell. Biol.* **9**:312–318 (1999) doi:10.1016/S0962-8924(99)01608-6.
35. D. Lechardeur, and G. L. Lukacs. Intracellular barriers to non-viral gene transfer. *Curr. Gene Ther.* **2**:183–194 (2002) doi:10.2174/1566523024605609.
36. R. Wang, and M. G. Brattain. The maximal size of protein to diffuse through the nuclear pore is larger than 60 kDa. *FEBS Lett.* **581**:3164–3170 (2007) doi:10.1016/j.febslet.2007.05.082.
37. P. L. Paine, and C. M. Feldherr. Nucleocytoplasmic exchange of Macromolecules. *Exp. Cell Res.* **74**:81–98 (1972) doi:10.1016/0014-4827(72)90483-1.
38. P. L. Paine. Nucleocytoplasmic movement of fluorescent tracers microinjected into living salivary gland cells. *J. Cell Biol.* **66**:652–657 (1975) doi:10.1083/jcb.66.3.652.

39. A. E. Smithand, and A. Helenius. How viruses enter animal cells. *Science*. **304**:237–242 (2004) doi:10.1126/science.1094823.
40. D. M. Shayakhmetov, A. M. Eberly, Z. Y. Li, and A. Lieber. Deletion of penton RGD motifs affects the efficiency of both the internalization and the endosome escape of viral particles containing adenovirus serotype 5 or 35 fiber knobs. *J. Virol.* **79**:1053–1061 (2005) doi:10.1128/JVI.79.2.1053-1061.2005.
41. E. M. van Damand, and W. Stoorvogel. Dynamin-dependent transferrin receptor recycling by endosome-derived clathrin-coated vesicles. *Mol. Biol. Cell.* **13**:169–182 (2002) doi:10.1091/mbc.01-07-0380.
42. M. Goldberg, R. Langer, and X. Jia. Nanostructured materials for applications in drug delivery and tissue engineering. *J. Biomater. Sci., Polym. Ed.* **18**:241–268 (2007) doi:10.1163/156856207779996931.
43. S. M. Moghimi, A. C. Hunter, and J. C. Murray. Long-circulating and target-specific nanoparticles: theory to practice. *Pharmacol. Rev.* **53**:283–318 (2001).
44. V. A. Sethuraman, M. C. Lee, and Y. H. Bae. A biodegradable pH-sensitive micelle system for targeting acidic solid tumors. *Pharm. Res.* **25**:657–666 (2008) doi:10.1007/s11095-007-9480-4.
45. D. Shenoy, S. Little, R. Langer, and M. Amiji. Poly(ethylene oxide)-modified poly(beta-amino ester) nanoparticles as a pH-sensitive system for tumor-targeted delivery of hydrophobic drugs: Part 2. *In vivo* distribution and tumor localization studies. *Pharm. Res.* **22**:2107–2114 (2005) doi:10.1007/s11095-005-8343-0.
46. S. Ganta, H. Devalapally, A. Shahiwala, and M. Amiji. A review of stimuli-responsive nanocarriers for drug and gene delivery. *J. Control. Release*. **126**:187–204 (2008) doi:10.1016/j.jconrel.2007.12.017.
47. H. Devalapally, D. Shenoy, S. Little, R. Langer, and M. Amiji. Poly(ethylene oxide)-modified poly(beta-amino ester) nanoparticles as a pH-sensitive system for tumor-targeted delivery of hydrophobic drugs: part 3. Therapeutic efficacy and safety studies in ovarian cancer xenograft model. *Cancer Chemother. Pharmacol.* **59**:477–484 (2007) doi:10.1007/s00280-006-0287-5.
48. A. Potineni, D. M. Lynn, R. Langer, and M. M. Amiji. Poly (ethylene oxide)-modified poly(beta-amino ester) nanoparticles as a pH-sensitive biodegradable system for paclitaxel delivery. *J. Control. Release*. **86**:223–234 (2003) doi:10.1016/S0168-3659(02)00374-7.